Inter-Organ Growth Coordination Is Mediated by the Xrp1-Dilp8 Axis in Drosophila

Laura Boulan, Ditte Andersen, Julien Colombani, Emilie Boone, Pierre Léopold

Inter-organ growth coordination is mediated by the Xrp1/Dilp8 axis in *Drosophila*

Laura Boulan[1,4], Ditte Andersen[2,3], Julien Colombani[2,3], Emilie Boone[2], Pierre Léopold[1,4,5]

[1] Institut Curie, PSL Research University, CNRS UMR3215, INSERM U934, UPMC Paris-Sorbonne, 26 Rue d'Ulm, 75005, Paris, France.

[2] Université Côte d'Azur, CNRS UMR7277, Inserm U1091, iBV, Parc Valrose, 06108, Nice, France.

[3] Current address: Department of Biology, Novo Nordisk Foundation Center for Stem Cell Biology (DanStem), University of Copenhagen, Copenhagen, Denmark.

[4] Correspondence: laura.boulan@curie.fr; pierre.leopold@curie.fr

[5] Lead contact

Keywords: organ growth, Dilp8, Drosophila, Minute, Xrp1, coordination, RpS12

ABSTRACT

How organs scale with other body parts is not mechanistically understood. We have addressed this question using the *Drosophila* imaginal disc model. When growth of one disc domain is perturbed, other parts of the disc and other discs slow down their growth, maintaining proper inter-disc and intra-disc proportions. We show here that the relaxin-like Dilp8 is required for this inter-organ coordination. Our work also reveals that the stress-response transcription factor Xrp1 plays a key role upstream of *dilp8* in linking organ growth status with non-autonomous/systemic growth response. In addition, we show that the small ribosomal subunit protein RpS12 is required to trigger Xrp1-dependent non-autonomous response. Our work demonstrates that RpS12, Xrp1 and Dilp8 constitute an independent regulatory module that ensures intra- and inter-organ growth coordination during development.

INTRODUCTION

Body size and organ proportions are important characteristics that define animal fitness, mobility, predation and competition for a given species. Animals adapt their growth and body size to environmental conditions, and the way the relative sizes of the different body parts is modified follows conserved allometric rules (Mirth et al., 2016), suggesting that coordination mechanisms are at play during development. Most recent studies on growth have focused on the mechanism of organ size determination without interrogating the complex question of coordinating growth between organs. One elegant way to tackle this question is to induce a local growth perturbation in a given organ and to analyze the non-autonomous/systemic responses triggered by this perturbation. This approach was recently used in mice where unilateral inhibition of proliferation in the limb cartilage reduces contralateral bone growth, thereby contributing to the maintenance of left/right bone symmetry (Roselló-Díez et al., 2018). In *Drosophila*, growth inhibition in the wing imaginal disc during larval development triggers a non-autonomous response reducing the growth rate of the leg or eye disc. As a consequence, the relative proportions between the slow-growing tissue and unperturbed tissues are maintained throughout development (Jaszczak and Halme, 2016; Parker and Shingleton, 2011). Growth coordination is also observed between different territories of the wing disc (Gokhale et al., 2016; Mesquita et al., 2010). Therefore, it seems that conserved mechanisms allow slow-growing tissues to systemically act on general growth parameters and maintain proportions between body parts. What signals mediate this inter-organ communication, and what molecular mechanisms link growth inhibition and signal production are currently open questions.

Here we show that the relaxin-like Dilp8 (Colombani et al., 2012; Garelli et al., 2012) is the signal that triggers the coordination of growth among organs during *Drosophila* development. Furthermore, we identify a novel pathway relying on the transcription factor Xrp1, which triggers Dilp8 expression in slow-growing tissues, allowing inter-organ coordination. The JNK and Hippo signaling pathways, both previously shown to regulate Dilp8, are not involved in this process. Our results also indicate that the

small ribosomal subunit protein RpS12 is required to trigger the Xrp1-dependent non-autonomous response.

RESULTS

Experimental setup

Imaginal discs grow extensively during the larval phase to form adult body parts after metamorphosis. In the wing imaginal disc, the pouch gives rise to the adult wing blade whereas the hinge and notum form the proximal and thorax structures, respectively (Figure 1A).

As an experimental setup to induce local growth perturbation in larval discs, we used the *pdm2^{R11F02}-Gal4* and the *nub-Gal4* lines to drive expression in the wing pouch. *pdm2^{R11F02}-Gal4* and *nub-Gal4* expression in the pouch starts early in disc development between the L2 and early L3 stages (Figure S1A). Lineage analysis using the G-TRACE technique (Evans et al., 2009) revealed that none of these drivers is expressed at earlier stages in the hinge+notum and the eye disc (Figure S1B). Since *nub-Gal4* is extensively expressed in the brain, we combined it with an *elav-GAL80* construct that prevents expression in most neurons (Figure S1C). *pdm2^{R11F02}-Gal4* (hereafter named *pdm2-Gal4*) drives minimal expression in the brain (Figure S1D) in three thermosensory neurons (Klein et al., 2015). The combination with an *elav-GAL80* construct prevents expression in these neurons (Figure S1D), therefore preventing any central effect of the driver.

Dilp8 is required to coordinate growth of imaginal tissues

In order to inhibit growth specifically in the wing pouch, we first used an RNAi line targeting a ribosomal protein (*UAS-RpL7^{RNAi}*). As expected, *pdm2>RpL7^{RNAi}* animals have smaller wing pouch territories at 4 days (90 hours AED) and 5 days (110 hours AED) of development, compared to control discs (Figure 1B-C). In these conditions, we also observed a non-autonomous inhibition of growth in the eye discs, indicative of inter-organ coordination (Figure 1D''). Notably, the hinge and the notum, two independent territories of the wing imaginal disc, also display coordinated growth reduction

(Figure 1B'). To quantify these non-autonomous responses, hereafter referred to as inter/intra-organ coordination (IOC), we chose to evaluate the hinge+notum, eye and pouch surfaces in our following experiments. Similar results were obtained with the *elavGa80, pdm2-Gal4* combination (Fig. S1E,E'), indicating that the non-autonomous effects observed are due to the pouch expression of the driver.

Since Dilp8 is (i) highly secreted in conditions of growth impairment (Figure 2A and S2A) and (ii) acting as an inhibitor of ecdysone production and tissue growth, we tested its role in IOC. RNAi-mediated inhibition of *dilp8* in the slow-growing wing pouch (*pdm2>Rpl7^{RNAi}, dilp8^{RNAi}*) fully rescued growth in the hinge and notum territories, but not in the pouch (Figure 1D,D'). This was confirmed using other genetic tools inducing similar growth perturbation *(elav-GAL80, nub>RpS3^{RNAi}*; Figure S1F-G). Notably, Dilp8 inhibition in the pouch also rescued growth of the eye disc (Figure 1D''), indicating that Dilp8 is required for growth coordination both within and between organs. In addition, overexpressing Dilp8 in the wing pouch non-autonomously reduces the size of the hinge and notum territories as well as the eye disc at the same developmental time (Figure 1E-E''). Feeding animals with 20E, the active form of ecdysone, significantly rescues growth inhibition in *pdm2>dilp8* animals (Figure S1H-H''), both autonomously and non-autonomously, suggesting that Dilp8 inhibits imaginal tissue growth by reducing ecdysone production. This overall indicates that Dilp8 acts as a systemic growth inhibitor and is a major effector of IOC.

Dilp8-mediated IOC is independent of JNK and Hippo signaling

What is the molecular mechanism linking growth perturbation to *dilp8* upregulation and the systemic growth response? The JNK pathway activates *dilp8* expression in the context of neoplastic growth (Colombani et al., 2012), or regenerative growth through JAK/STAT signaling (Katsuyama et al., 2015), while the Hippo pathway controls *dilp8* expression in physiological conditions to buffer growth-associated developmental noise (Boone et al., 2016). Neither inhibition of JNK signaling nor of Hippo signaling could rescue the upregulation of *dilp8* mRNA levels observed at 110 hours AED (*elav-GAL80, nub>RpS3^{RNAi}*) (Figure 2A). However, we noticed a partial rescue of the developmental

delay at pupariation upon JNK and Hippo inhibition, suggesting that these signaling pathways could play a role after 110 hours AED to time pupariation (Figure 2B). According to these results, inhibition of JNK or Hippo signaling was not able to rescue tissue growth, neither autonomously (wing pouch) nor non-autonomously (hinge + notum) (Figure 2C,C').

Additional regulators of *dilp8* transcription include EcR (Zhang et al., 2015) and PERK/ATF4 signaling in response to ER stress (Demay et al., 2014). However, silencing these pathways in *Rp-RNAi* discs does not rescue non-autonomous growth inhibition (Figure S2B). Therefore, none of the regulatory pathways known to trigger *dilp8* expression is involved in the response to local growth perturbation.

Xrp1 controls IOC upstream of Dilp8

Dilp8 was identified in a genome-wide genetic screen for genes involved in the developmental delay induced by growth impairment in the imaginal discs (Colombani et al., 2012). A gene called *xrp1,* encoding a bZIP transcription factor, also came out of this initial screen. Although poorly rescuing the delay induced by neoplastic growth (*elav-GAL80, rn>avl*^{RNAi}, data not shown), silencing *xrp1* efficiently rescues the developmental delay induced by slow-growing discs (*elav-GAL80, nub>Rps3*^{RNAi}; Figure 2B), and, accordingly, the levels of *dilp8* mRNA (Figure 2A). Consistent with the rescue of *dilp8* expression levels, we observe a full rescue of non-autonomous (hinge+notum) growth in *elav-GAL80, nub>RpS3*^{RNAi}*, xrp1*^{RNAi} animals (Figure 2C' and S2C'), with little or no effect on autonomous (pouch) growth (Figure 2C and S2C). Non-autonomous rescue of growth and of developmental delay was also observed in homozygous *xrp1* mutant animals (Figure 2D-E) (Akdemir et al., 2007). Taken together, these results indicate that the bZIP transcription factor Xrp1 is required upstream of Dilp8 in slow-growing tissues to trigger inter- and intra-organ growth coordination.

We also observe an increase in cell death in *nub>RpS3*^{RNAi} wing pouches, but not in the neighboring tissue. The simultaneous downregulation of *xrp1* prevents autonomous cell death to the same extent as the expression of the caspase inhibitor p35 (Figure S2D,D'). Yet, inhibition of cell death in *Rp-RNAi* discs (*elav-GAL80, nub>RpS3*^{RNAi}*, >p35*) has a mild effect on growth and does not phenocopy the non-

autonomous rescue obtained by *Xrp1* silencing (Figure S2E,E'). Therefore Xrp1 induces autonomous cell death in Rp-RNAi tissues, but this apoptotic induction is not responsible for the general growth inhibition induced by the *nub>RpS3*^{RNAi} condition.

Xrp1 overexpression is sufficient to trigger non-autonomous reduction of tissue growth

Xrp1 has previously been implicated in the response to genotoxic stress (irradiation), the maintenance of genome integrity downstream of p53 (Akdemir et al., 2007) and during P-element dysgenesis (Francis et al., 2016). In order to gain insights into its putative growth-related function, we generated transgenic animals expressing the short and the long isoforms of Xrp1 under *UAS* control (*UAS-xrp1-S* and *UAS-xrp1-L*). Either of the two transgenes expressed in the wing pouch induces apoptosis and important reduction of autonomous tissue size (Figure 3A and S3A). This is accompanied by non-autonomous growth inhibition in the neighboring territories -hinge and notum- as well as in the eye disc (Figure 3A',A''). Accordingly, in these conditions, *dilp8* mRNA levels is upregulated (Figure 3B). As observed in *pdm2>Rp*^{RNAi} discs, silencing *dilp8* in *pdm2>xrp1-L* conditions has no autonomous effect but fully rescues non-autonomous growth inhibition (Figure 3C,C'). This condition did not rescue apoptosis in the pouch (Figure S3A), suggesting that Dilp8 only mediates non-autonomous growth effects of Xrp1. These results indicate that Xrp1 is sufficient to induce IOC and confirm that Dilp8 is required downstream of Xrp1 in this process.

In order to better understand the link between local growth perturbation and Xrp1 function, we analyzed *xrp1* expression in IOC conditions. We observed a modest but consistent upregulation of the *xrp1-lacZ* reporter in *pdm2>Rps3*^{RNAi} pouches (Figure S3B, compare β-Gal accumulation inside and outside of the pouch domain). This result was confirmed by qRT-PCR on dissected wing imaginal discs, with primers detecting either a common region to the long and the short isoforms, or only the long one (Figure S3C). These results suggest either that a fine-tuned transcriptional regulation of Xrp1 is sufficient to trigger *dilp8* expression and IOC, or that Xrp1 is regulated at post-transcriptional levels.

Finally, we tested whether Dilp8/Xrp1 signaling responds to a broader type of growth perturbation than *Rp-RNAi* growth inhibition. We noted that inhibiting growth by acting on insulin- or Hippo-signaling does not trigger IOC (Figure S3D-D''). However, silencing the growth activator dMyc triggers IOC and a delay at pupariation (Figure S3E-F). Interestingly, these systemic responses are abolished by silencing *dilp8* or *xrp1* (Figure S3E-F). Therefore, our results indicate that Dilp8/Xrp1 signaling ensures non-autonomous growth feedback in several situations of local growth perturbation.

A role for the atypical ribosomal protein RpS12 in IOC

What could be the growth sensor upstream of Xrp1 in slow-growing tissues? Xrp1 was recently found in a screen for genes involved in cell competition induced by *Minute* mutations (Lee et al., 2016). *Minute* cells are heterozygous mutant for genes encoding ribosomal protein, a context presenting some similarities with the RNAi-mediated silencing of *RpL7* and *RpS3* that we used to inhibit growth. The only upstream regulator of Xrp1 known so far is p53. p53 is required to induce *xrp1* upon irradiation (Akdemir et al., 2007) and was more recently shown to control growth coordination between compartments (Mesquita et al., 2010). In addition, previous work has shown that *xrp1* could respond to oxidative stress (Gruenewald et al., 2009), and that both oxidative stress and Nrf2 are linked to *Minute*-induced cell competition (Kucinski et al., 2017). However, we find that RNAi-mediated downregulation of *p53* or inhibition of oxidative stress signaling (*UAS-CAT+SOD*, *UAS-nrf2*^{RNAi}) in slow-growing discs produces no or only minor rescue of non-autonomous growth (Figure S2B). Although potentially suggestive of a partial contribution of these pathways in IOC, these data point to another mode of regulation for Xrp1 in this context.

Another potential candidate for this regulation is the atypical ribosomal protein RpS12, since it plays a role in Minute-induced cell competition (Kale et al., 2018). Consistent with its function as a ribosomal protein, silencing RpS12 in the wing pouch (*pdm2>rpS12*^{RNAi}) leads to a strong autonomous inhibition of tissue growth (Figure 4A). Yet, in contrast to the downregulation of *RpS3* and *RpL7*, *RpS12* silencing does not induce IOC (Figure 4A',A''), suggesting that it is itself involved in this

process. Indeed, the downregulation of *RpS12* in *pdm2>RpL7*^{RNAi} pouches rescues growth non-autonomous inhibition (hinge+notum and eye disc, Figure 4A',A''), although it has no autonomous effect (wing pouch, Figure 4A). Similar results were obtained in *elav-GAL80, nub>RpS3*^{RNAi}*, rpS12*^{RNAi} animals (Figure S4A). These observations indicate that RpS12 itself is required for IOC induced by *Rp* gene silencing. Consistent with Dilp8 being the effector for IOC, minor upregulation of Dilp8 is observed in *pdm2>rpS12*^{RNAi} discs, while the up-regulation of Dilp8 in *pdm2>RpL7*^{RNAi} discs is rescued by silencing *rpS12* (Figure 4B).

In order to strengthen the epistasis between RpS12, Xrp1 and Dilp8, we first silenced *xrp1* in discs overexpressing *dilp8*. No effect was observed on *dilp8*-induced autonomous and non-autonomous growth inhibition, confirming that Dilp8 acts downstream of Xrp1 (Figure S4B,B'). In parallel, the downregulation of *rpS12* in *xrp1*-overexpressing discs has little or no effect on Xrp1-induced growth inhibition (Figure S4B,B'), suggesting that Xrp1 acts downstream of RpS12. Collectively, these results suggest that Rps12 functions as a sensor of ribosomal protein function upstream of Xrp1 and Dilp8 for the control of IOC.

DISCUSSION

Dilp8 controls systemic growth

Dilp8 is secreted by growing, regenerating and tumorous tissues. It acts remotely on steroid hormone production to delay the transition to the pupal stage when growth is impaired. In this work, we show that the induction of *dilp8* by slow-growing discs is necessary and sufficient to trigger remote growth inhibition in other disc domains and other discs, thereby contributing to maintaining proper body proportions. These results establish that Dilp8 is a key regulator of the systemic response to a local growth perturbation, acting both by delaying the developmental transition and by coordinating growth between organs.

Several lines of evidence indicate that Dilp8-mediated IOC requires the modulation of ecdysone levels. First, Dilp8 overexpression inhibits tissue growth through a systemic relay involving Lgr3-

positive neurons that connect, via PTTH neurons, to the prothoracic gland where ecdysone is produced (Colombani et al., 2015). Second, ecdysone was shown to promote growth of imaginal tissues (Delanoue et al., 2010; Dye et al., 2017; Herboso et al., 2015; Jaszczak et al., 2015). Third, feeding larvae with ecdysone prevents IOC (Parker and Shingleton, 2011). Here we reinforce this hypothesis by showing that 20E supply rescues growth inhibition caused by *dilp8* overexpression both autonomously and non-autonomously. This suggests that Dilp8 inhibits tissue growth via this systemic relay.

We observe that driving *Rp-RNAi* in the wing pouch leads to pupal lethality (data unshown). We show here, as well as in previous studies, that this manipulation triggers a non-autonomous, systemic response leading to a strong inhibition of ecdysone biosynthesis. We do not know how this response is controlled in time but one possibility is that the systemic response also interferes with the control of ecdysone production during some key steps of metamorphosis, leading to pupal lethality.

A different pathway controlling Dilp8-dependent growth coordination

Two independent pathways have previously been shown to trigger *dilp8* expression in response to modifications of the growth status. In neoplastic growth conditions, the JNK pathway is a strong inducer of Dilp8 and inhibits the larval-pupal transition in response to developing tumors (Colombani et al., 2012). Additionally, the transcriptional effector of Hippo signaling, Yorkie/Scalloped, modulates the Dilp8 promoter to couple normal growth and *dilp8* expression (Boone et al., 2016). We show here that none of these pathways is responsible for *dilp8* induction in response to growth inhibition in *Rp-RNAi* tissues. Instead, an independent pathway triggered by Xrp1 is potently activated in these conditions, leading to a strong induction of *dilp8*.

Therefore, different types of growth perturbations (minor growth defects due to developmental variability, neoplastic growth, irradiation, growth inhibition in Minute conditions) converge on the regulation of Dilp8 to trigger systemic responses, but use selective, independent pathways to do so.

This potentially allows organisms to finely tune local and systemic responses according to the type of growth impairment.

Xrp1 is a growth inhibitor

Xrp1 was previously involved in genotoxic stress (irradiation) response, and the maintenance of genome integrity downstream of p53 (Akdemir et al., 2007) and during P-element dysgenesis (Francis et al., 2016). Our results uncover another function for Xrp1 as a growth regulator. The knock-down of *xrp1* in *Rp-RNAi* discs revealed that it is required for non-autonomous growth inhibition through Dilp8 induction. However, when Rp genes are silenced, removal of Xrp1 is not sufficient to rescue growth autonomously. By contrast, *xrp1* overexpression inhibits tissue growth both autonomously and non-autonomously, and only the non-autonomous response relies on Dilp8. Our study of IOC sheds new light on the biology of Xrp1, demonstrating that Xrp1 carries two independent functions in growth control. On one hand, Xrp1 autonomously inhibits tissue growth and triggers apoptosis. This is in line with previous results showing that Xrp1 is sufficient to inhibit cell proliferation in S2 cells (Akdemir et al., 2007), in eye discs (Tsurui-Nishimura et al., 2013), and with the Xrp1-dependent induction of apoptosis we observed in *Rp-RNAi* tissues or upon *xrp1* overexpression in the wing pouch. On the other hand, activation of Xrp1 signaling in *Rp-RNAi* discs or upon overexpression remotely inhibits tissue growth in a Dilp8-dependent manner.

Rps12 as a sensor for ribosomal protein function

Whether the Xrp1 pathway is activated in *Rp-RNAi* discs by a general reduction of protein translation and/or growth potential, or by a specific pathway such as the ribosomal stress response, is unclear. Our finding that RpS12 is required for IOC and Dilp8 upregulation in *Rp-RNAi* discs brings insights into this mechanism. RpS12 is one of the last ribosomal proteins assembled into the small ribosomal subunit and, in contrast to most *Drosophila* Rp-encoding genes, *rpS12* is not haplo-insufficient (Marygold et al., 2007). Kale et al. recently established that RpS12 is required to trigger Minute cell competition, and that the relative levels of RpS12 define cell competitiveness. Moreover, recent data

from Baker's group indicates that RpS12 is required for *xrp1* expression in Minute clones (Lee et al., 2018). We bring here the remarkable finding that removing RpS12, while inducing autonomous growth inhibition by itself, rescues the Xrp1/Dilp8 non-autonomous response in the context of already *Rp-RNAi* discs. This is indeed strong evidence that Rps12 is itself required for the cells to respond to a defect in Rp protein function. We therefore propose a model whereby RpS12 acts as an upstream signal for IOC upon dis-function of ribosomal proteins (RpS3 or RpL7 in this study). RpS12 is required for Xrp1 activation and *dilp8* upregulation, ultimately leading to systemic response and IOC (Figure 4C). This raises the interesting possibility that ribosomal protein function is used by cells and tissue as a proxy for their growing status and, as such, participates in inter-organ growth coordination mechanisms.

Xrp1, cell competition and size adjustment

Two recent studies report that Xrp1 is required in Minute clones to induce cell competition by surrounding wild-type cells (Baillon et al., 2018; Lee et al., 2018). This work reveals that Xrp1 mediates most of the changes in gene expression and translation inhibition observed in Minute cells. Lee et al. also report a mild transcriptional increase of *xrp1* in heterozygous Minute cells, independently of p53. This suggests similarities for the induction of Xrp1 signaling in the context of cell competition and in inter-organ growth coordination. Our finding that Xrp1 is required in *Rp-RNAi* pouch for non-autonomous growth inhibition, but only marginally for autonomous growth reduction in the pouch domain (see our Figures 2C and S2C), is consistent with the observations by Baillon et al., 2018 that Minute clones mutant for *xrp1* are still 40 to 60% smaller than wild-type twin clones. This suggests that the undergrowth of Minute or *Rp-RNAi* cells is in part due to an Xrp1-independent mechanism. Finally, our findings showing that Xrp1 triggers systemic responses raise the possibility that systemic signals could also contribute to local cell competition.

AUTHORS CONTRIBUTIONS

Conceptualization: LB and PL, Methodology: LB and PL, Formal analysis: LB, Investigation: LB, DA, JC and EB, Writing original draft: LB and PL, Writing review & editing: LB, DA, JC, EB and PL, Visualization: LB, Supervision: PL, Project Administration: PL, Funding acquisition: PL.

DECLARATION OF INTERESTS

The authors declare no competing interests.

ACKNOWLEDGEMENTS

We thank T. Pihl, J. Villalba, J. Marcetteau, L. Ruel and L. Barrio for help with the experiments and all members of the laboratory for insightful discussions; M. Milan, K. Basler, the Bloomington Stock Center and the Vienna Drosophila RNAi Center for fly stocks; K. Basler, D. Lubensky, N. Baker, M. Milan, J-P. Vincent for discussions. This project has received funding from the Association pour la recherche sur le cancer (grant n°PGA120150202355 to P.L. and fellowship n°PDF20141202140 to L.B.), Inserm, CNRS, the European Research Council (ERC Advanced grant n°268813 to P.L.), the Labex Signalife program (grant ANR-11-LABX-0028-01 to P.L.), the Marie Sklodowska-Curie Actions (fellowship n°657685 to L.B.).

REFERENCES

Akdemir, F., Christich, a., Sogame, N., Chapo, J., and Abrams, J.M. (2007). p53 directs focused genomic responses in Drosophila. Oncogene *26*, 5184–5193.

Baillon, L., Germani, F., Rockel, C., Hilchenbach, J., and Basler, K. (2018). Xrp1 is a transcription factor required for cell competition-driven elimination of loser cells. Sci. Rep. *8*, 17712.

Boone, E., Colombani, J., Andersen, D.S., and Léopold, P. (2016). The Hippo signalling pathway coordinates organ growth and limits developmental variability by controlling dilp8 expression. Nat.

Commun. *7*, 13505.

Colombani, J., Andersen, D.S., and Léopold, P. (2012). Secreted peptide Dilp8 coordinates Drosophila tissue growth with developmental timing. Science *336*, 582–585.

Colombani, J., Andersen, D.S., Boulan, L., Boone, E., Romero, N., Virolle, V., Texada, M., and Léopold, P. (2015). Drosophila Lgr3 Couples Organ Growth with Maturation and Ensures Developmental Stability. Curr. Biol. *25*.

Delanoue, R., Slaidina, M., and Leopold, P. (2010). The steroid hormone ecdysone controls systemic growth by repressing dMyc function in Drosophila fat cells. Dev Cell *18*, 1012–1021.

Demay, Y., Perochon, J., Szuplewski, S., Mignotte, B., and Gaumer, S. (2014). The PERK pathway independently triggers apoptosis and a Rac1/Slpr/JNK/Dilp8 signaling favoring tissue homeostasis in a chronic ER stress Drosophila model. Cell Death Dis. *5*, e1452-10.

Dye, N.A., Popović, M., Spannl, S., Etournay, R., Kainmüller, D., Ghosh, S., Myers, E.W., Jülicher, F., and Eaton, S. (2017). Cell dynamics underlying oriented growth of the Drosophila wing imaginal disc. Development *144*, 4406–4421.

Evans, C.J., Olson, J.M., Ngo, K.T., Kim, E., Lee, N.E., Kuoy, E., Patananan, A.N., Sitz, D., Tran, P.T., Do, M.T., et al. (2009). G-TRACE: Rapid Gal4-based cell lineage analysis in Drosophila. Nat. Methods *6*, 603–605.

Francis, M.J., Roche, S., Cho, M.J., Beall, E., Min, B., Panganiban, R.P., and Rio, D.C. (2016). *Drosophila* IRBP bZIP heterodimer binds P-element DNA and affects hybrid dysgenesis. Proc. Natl. Acad. Sci. *113*, 13003–13008.

Garelli, A., Gontijo, A.M., Miguela, V., Caparros, E., and Dominguez, M. (2012). Imaginal discs secrete insulin-like peptide 8 to mediate plasticity of growth and maturation. Science *336*, 579–582.

Gokhale, R.H., Hayashi, T., Mirque, C.D., and Shingleton, A.W. (2016). Intra-organ growth coordination in Drosophila is mediated by systemic ecdysone signaling. Dev. Biol. *418*, 135–145.

Gruenewald, C., Botella, J. a., Bayersdorfer, F., Navarro, J. a., and Schneuwly, S. (2009). Hyperoxia-induced neurodegeneration as a tool to identify neuroprotective genes in Drosophila melanogaster. Free Radic. Biol. Med. *46*, 1668–1676.

Herboso, L., Oliveira, M.M., Talamillo, A., Pérez, C., González, M., Martín, D., Sutherland, J.D., Shingleton, A.W., Mirth, C.K., and Barrio, R. (2015). Ecdysone promotes growth of imaginal discs through the regulation of Thor in D. melanogaster. Sci. Rep. *5*, 12383.

Jaszczak, J.S., and Halme, A. (2016). Arrested development: coordinating regeneration with development and growth in Drosophila melanogaster. Curr. Opin. Genet. Dev. *40*, 87–94.

Jaszczak, J.S., Wolpe, J.B., Dao, A.Q., and Halme, A. (2015). Nitric oxide synthase regulates growth coordination during Drosophila melanogaster imaginal disc regeneration. Genetics.

Kale, A., Ji, Z., Kiparaki, M., Blanco, J., Rimesso, G., Flibotte, S., and Baker, N.E. (2018). Ribosomal Protein S12e Has a Distinct Function in Cell Competition. Dev. Cell *44*, 42–55.e4.

Katsuyama, T., Comoglio, F., Seimiya, M., Cabuy, E., and Paro, R. (2015). During Drosophila disc regeneration, JAK/STAT coordinates cell proliferation with Dilp8-mediated developmental delay. Proc. Natl. Acad. Sci. U. S. A. *112*, E2327-36.

Klein, M., Afonso, B., Vonner, A.J., Hernandez-Nunez, L., Berck, M., Tabone, C.J., Kane, E.A., Pieribone, V.A., Nitabach, M.N., Cardona, A., et al. (2015). Sensory determinants of behavioral dynamics in Drosophila thermotaxis. Proc. Natl. Acad. Sci. *112*, E220–E229.

Kucinski, I., Dinan, M., Kolahgar, G., and Piddini, E. (2017). Chronic activation of JNK JAK/STAT and oxidative stress signalling causes the loser cell status. Nat. Commun.

Lee, C.-H., Rimesso, G., Reynolds, D.M., Cai, J., and Baker, N.E. (2016). Whole-Genome Sequencing and iPLEX MassARRAY Genotyping Map an EMS-induced Mutation Affecting Cell Competition in Drosophila melanogaster. G3 *6*, 3207–3217.

Lee, C.-H., Kiparaki, M., Blanco, J., Folgado, V., Ji, Z., Kumar, A., Rimesso, G., and Baker, N.E. (2018). A

Regulatory Response to Ribosomal Protein Mutations Controls Translation, Growth, and Cell Competition. Dev. Cell *46*, 1–14.

Marygold, S.J., Roote, J., Reuter, G., Lambertsson, A., Ashburner, M., Millburn, G.H., Harrison, P.M., Yu, Z., Kenmochi, N., Kaufman, T.C., et al. (2007). The ribosomal protein genes and Minute loci of Drosophila melanogaster. Genome Biol. *8*.

Mesquita, D., Dekanty, A., and Milán, M. (2010). A dp53-dependent mechanism involved in coordinating tissue growth in Drosophila. PLoS Biol. *8*, e1000566.

Mirth, C.K., Anthony Frankino, W., and Shingleton, A.W. (2016). Allometry and size control: what can studies of body size regulation teach us about the evolution of morphological scaling relationships? Curr Opin Insect Sci *13*, 93-98.

Parker, N.F., and Shingleton, A.W. (2011). The coordination of growth among Drosophila organs in response to localized growth-perturbation. Dev. Biol. *357*, 318–325.

Roignant, J.Y., Carré, C., Mugat, B., Szymczak, D., Lepesant, J.A., and Antoniewski, C. (2003). Absence of transitive and systemic pathways allows cell-specific and isoform-specific RNAi in Drosophila. RNA.

Roselló-Díez, A., Madisen, L., Bastide, S., Zeng, H., and Joyner, A.L. (2018). Cell-nonautonomous local and systemic responses to cell arrest enable long-bone catch-up growth in developing mice. PLoS Biol. *16*, e2005086.

TSURUI-NISHIMURA, N., NGUYEN, T.Q., KATSUYAMA, T., MINAMI, T., FURUHASHI, H., OSHIMA, Y., and KURATA, S. (2013). Ectopic Antenna Induction by Overexpression of CG17836/Xrp1 Encoding an AT-Hook DNA Binding Motif Protein in Drosophila. Biosci. Biotechnol. Biochem. *77*, 339–344.

Zhang, C., Robinson, B.S., Xu, W., Yang, L., Yao, B., Zhao, H., Byun, P.K., Jin, P., Veraksa, A., and Moberg, K.H. (2015). The Ecdysone Receptor Coactivator Taiman Links Yorkie to Transcriptional Control of Germline Stem Cell Factors in Somatic Tissue. Dev. Cell *34*, 168–180.

FIGURES LEGENDS

Figure 1. Dilp8 mediates growth coordination in response to local growth perturbations

(A) Scheme of a wing imaginal disc showing the different territories used to assess tissue growth. (B,B') Area measurements of the wing pouch (autonomous; B) and hinge and notum (non-autonomous; B') in control wing discs (*pdm>GFP^{RNAi}*) and *Rp-RNAi* wing discs (*pdm2>RpL7^{RNAi}*), showing the coordination of growth between slow-growing tissues and other imaginal tissues at 90h and 110h AED (n≥29; *** p<0.001, t-tests). (C) Representative pictures of wing imaginal discs of the two genotypes stained for Wingless (Wg), illustrating the coordinated reduction in area size of wing and notum/hinge in *pdm2>RpL7^{RNAi}* animals. (D-E'') Area measurement of the wing pouch (D and E), the adjacent disc territories (hinge and notum; D' and E') and a remote organ (eye disc; D'' and E'') in animals of the different genotypes at 110h AED. (E-E'') The downregulation of *dilp8* in *pdm2>RpL7^{RNAi}* animals (*pdm2>RpL7^{RNAi}, dilp8^{RNAi}*) has a very mild effect on the size of the wing pouch but fully rescues growth non-autonomously (n≥48; *** p<0.001, ** p<0.01 and ns=not significant, ANOVA). (E-E'') *dilp8* overexpression in the wing pouch (*pdm2>dilp8*) triggers both autonomous and non-autonomous inhibition of tissue growth (n≥26; (*** p<0.001, t-tests). Data are represented as mean ± SEM. See also Figure S1.

Figure 2. Removal of *xrp1* in *Rp-RNAi* discs reduces *dilp8* levels and prevents growth coordination

(A) Measurement of *dilp8* mRNA levels by qRT-PCR on whole larvae of the indicated genotypes. (B) Pupariation curve showing a full rescue of the delay at pupariation upon knock-down of *xrp1* in the pouch. Percentage of larvae that have pupariated at the indicated

hours AED is shown (n≥53). (C,C') Measurement of pouch area (C) and hinge and notum area (C') in wing discs of the indicated genotypes, showing a rescue of the hinge+notum territories upon knock-down of *xrp1* in *Rp-RNAi* wing pouch. Inhibiting JNK or Hpo signaling does not rescue tissue growth (n≥34). (D,D') Measurement of pouch area (D) and hinge and notum area (D´) in wing discs of the indicated genotypes, showing a rescue of the hinge+notum territories in a *xrp1* mutant background (n≥17). (A, C-C´´, D-D´´) Experiments were done at 110h AED. Data are represented as mean ± SEM (*** p<0.001 and ns=not significant, ANOVA). (E) Pupariation curve showing a rescue of the delay at pupariation of *Rp-RNAi* (*pdm2>RpS3*^{RNAi}) animals in a *xrp1* mutant background. Percentage of larvae that have pupariated at the indicated hours AED is shown (n≥71). See also Figure S2.

Figure 3. Non-autonomous growth inhibition by Xrp1 is mediated by Dilp8

(A-A'') Measurement of wing pouch area (A), hinge and notum area (A') and area of a remote organ (eye disc; A'') in animals of the indicated genotypes. Overexpression of the short (*UAS-xrp1-S*) and long (*UAS-xrp1-L*) isoforms of *xrp1* in the wing pouch inhibits tissue growth and triggers inter-organ growth coordination (n≥16). (B) *xrp1* overexpression in the wing pouch upregulates *dilp8* mRNA levels, as measured by qRT-PCR on whole larvae (*** p<0.001, t-test). (C,C') Measurement of wing pouch area (C), hinge and notum area (C') in wing discs of the indicated genotypes, showing that Dilp8 is required for the non-autonomous, but not the autonomous, effects of *xrp1* overexpression (n≥15). (A-C) All experiments were done at 110h AED. Data are represented as mean ± SEM (*** p<0.001 and ns=not significant, ANOVA). See also Figure S3.

Figure 4. RpS12 is required for *dilp8* induction and systemic growth inhibition

(A-A'') Measurement of wing pouch area (A), area of neighboring territories (hinge and notum; A') and area of a remote organ (eye disc; A'') in animals of the indicated genotypes at 110h AED, showing that the knock-down of RpS12 in *Rp-RNAi* wing pouch rescues tissue growth in a non-autonomous manner (n≥21). The downregulation of *rpS12* alone strongly reduces tissue growth autonomously (A) but does not trigger inter-organ coordination (A', A''). Data are represented as mean ± SEM (*** p<0.001 and ns=not significant, ANOVA). (B) Dilp8 staining in wing imaginal discs of the indicated genotypes at 110h AED, showing the rescue of Dilp8 levels in *pdm2>RpL7^{RNAi}, rpS12^{RNAi}* discs compared to *pdm2>RpL7^{RNAi}* discs. (C) A model for the RpS12/Xrp1/Dilp8 regulatory pathway triggering IOC in response to local growth perturbation. See also Figure S4.

STAR METHODS

CONTACT FOR REAGENT AND RESOURCE SHARING

Further information and requests for resources and reagents should be directed to and will be fulfilled by the Lead Contact, Pierre Léopold (pierre.leopold@curie.fr).

EXPERIMENTAL MODEL AND SUBJECT DETAILS

Drosophila strains and maintenance

The following strains were provided by the Bloomington Drosophila Stock Center (BDSC): *pdm2^{R11F02}-Gal4* (49828), *UAS-GFP^{RNAi}* (35786), *UAS-CAT* (24621), *UAS-SOD$^{12.1}$* (33605), *xrp1-lacZ* (11569), *UAS-bsk^{DN}* (6409), *Df(3R)Exel6181* (7660), *Df(3R)Exel6182* (7661), *UAS-dMyc^{RNAi} (36123), UAS-xrp1^{RNAi}* (34521), UAS-p35 (5072), G-TRACE (28280). The following strains were

provided by the Vienna Drosophila RNAi Center (VDRC): *UAS-RpS3*^{RNAi} (37741), *UAS-RpL7*^{RNAi} (21973), *UAS-dilp8*^{RNAi} (102604), *UAS-tak1*^{RNAi} (101357), *UAS-yki*^{RNAi} (104523), *UAS-xrp1*^{RNAi} (107860 used in all experiments except if mentioned, 33010), *UAS-sd*^{RNAi} (101497), *UAS-p53*^{RNAi} (38235), *UAS-nrf2*^{RNAi} (108127), *UAS-mafS*^{RNAi} (109303), *UAS-p38*^{RNAi} (102484), *UAS-GCN2*^{RNAi} (103976), *UAS-PERK*^{RNAi} (110278), *UAS-rpS12*^{RNAi} (109381), *UAS-PI3K*^{RNAi} (38985), *UAS-inR*^{RNAi} (992). *nub-Gal4* (Azpiazu and Morata, 2000), *UAS-dilp8* (Colombani et al., 2012) and *UAS-EcR*^{RNAi} (Roignant et al., 2003) were as described. The *elav-GAL80* was kindly provided by Alex Gould (The Francis Crick Institute).

Flies were reared and experiments were performed on fly food containing, per liter: 34g inactivated yeast powder, 83g corn flour, 10g agar and 3.5g Moldex. Experiments were done at 25°C. For all experiments, both males and females were used.

For all experiments, a precise staging of the animals was done with 4-hours egg layings collected on agar plates with yeast. The next day, recently hatched L1 larvae were collected 24 hours AED and reared in tubes (forty larvae each) containing standard food. The developmental stage or time of development at which analysis were done is indicated in figure legends for all experiments.

METHOD DETAILS

Immunohistochemistry

Tissues were dissected in 1X phosphate-buffered saline (PBS) at the indicated hours after egg deposition (AED), fixed in 4% formaldehyde (Sigma) in PBS for 20 minutes at room temperature, washed in PBS containing 0.1% Triton-X-100 (PBT), blocked in PBT containing 10% fetal bovine serum and incubated overnight with primary antibodies at 4 °C. The next day, tissues were washed, blocked again and incubated with secondary antibodies at 1/400

dilution for 2 hours at room temperature. After washing, tissues were mounted in Vectashield containing DAPI for staining of DNA (Vector Labs).

The following primary antibodies were used: mouse anti-Wingless (Wg; concentrated 4D4 from DSHB; 1/200), rabbit anti-cleaved Caspase 3 (Casp3*; Cell Signaling; 1/100), chicken anti-beta-galactosidase (β-Gal; GeneTex; 1/1000), rat anti-Dilp8 (Colombani et al., 2012; 1/500), rabbit anti-cleaved Dcp1 (Cell Signaling; 1/100). The following secondary antibodies were used: Alexa Fluor 488 goat anti-mouse, Alexa Fluor 546 goat anti-mouse, Alexa Fluor 645 goat anti-mouse, Alexa Fluor 546 goat anti-rabbit, Alexa Fluor 546 goat anti-rat, Alexa Fluor 488 goat anti-chicken.

Imaging and quantifications

Fluorescence images were acquired using a Leica SP5 DS confocal microscope and processed using Adobe Photoshop CS5 or Fiji (Schindelin et al., 2012). Wg staining was used to measure area of the different territories in the wing imaginal discs: the inner ring of Wg was used to define the wing pouch area, and the rest of the wing disc was defined as hinge+notum territories.

For Dilp8 stainings, z stacks of 10µm (0,29µm/slice) were acquired starting on the apical side of the wing discs and presented as maximal projections. For G-TRACE, Dcp1 and brains visualization, z stacks of dissected tissues with a 0,45µm step were acquired and presented as maximal projections. For quantification of apoptosis, the Dcp1-positive area was determined for each territory using Fiji and normalized to the area of the territory for each disc.

Pupariation curves

4-hours egg layings were collected on agar plates with yeast. L1 larvae were collected at 24 hours AED and reared in tubes (forty larvae each) containing standard food (see above). The

number of larvae that had pupariated was scored at the indicated time points AED.

20E treatment

For 20E treatments, L1 larvae synchronized at 24h AED were transferred into tube with standard medium and yeast paste daily supplemented with 0.2 or 0.5 mg/ml 20-hydroxyecdysone (Sigma) until dissection at 110h AED. A stock solution of 20E diluted in ethanol at 5mg/ml was used and diluted in PBS for the experiments. Ethanol alone was used as a control. The concentration of ethanol is constant in all conditions.

Quantitative RT-PCR

Larvae were collected at the indicated number of hours AED. Whole larvae or dissected wing discs were frozen in liquid nitrogen. Total RNA was extracted using a QIAGEN RNeasy Lipid Tissue Mini Kit (for whole larvae) or a QIAGEN RNeasy Micro Kit (for dissected wing discs) according to the manufacturer's protocol. RNA samples (2-3µg per reaction) were treated with DNase and reverse-transcribed using SuperScript II reverse transcriptase (Invitrogen), and the generated cDNAs were used for real-time PCR (StepOne Plus, Applied Biosystems) using PowerSYBRGreen PCR mastermix (Applied Biosystems). Samples were normalized to the levels of the ribosomal protein rp49 transcript levels and fold changes were calculated using the ΔΔCt method. Three separate biological samples were collected for each experiment and triplicate measurements were performed. The following primers were used: rp49-sense: 5'-CTT CAT CCG CCA CCA GTC-3', rp49-antisense: 5'-CGA CGC ACT CTG TTG TCG-3' (Slaidina et al., 2009), dilp8-sense: 5'-CGA CAG AAG GTC CAT CGA GT-3', dilp8-antisense: 5'-GTT TTG CCG GAT CCA AGT C-3', xrp1-L-sense: 5'-TCA TTG TTT CTT TCT AAC GGT CAA-3', xrp1-L-antisense: 5'- GGT TGC TGT TGT TTG ATT CG-3', xrp1-common-sense: 5'-GAC CAC ACC GGA GAT TAT CAA-3', xrp1-common-antisense: 5'-GCT GGT ACT GGT ACT TGT GGT G-3'.

Xrp1 cloning.

The sequence encoding the long form of Xrp1 (Xrp1-L; amino acids 1-668) was PCR amplified from the BDGP EST cDNA clone SD01985 and cloned into the pENTR/D-TOPO vector using the following primers: sense: 5'-CAC CAT GAT CCA GGA GCC AGC ACG AGT A-3' and antisense: 5'-TCA GTC CTG CTC CTG CTT AAC GTA AG-3' (with stop codon). Sequence analysis detected a number of mutations in the SD01985 clone (according to the reference genome assembly for *D. melanogaster*) that were corrected using the QuickChange Multi site-directed mutagenesis kit (Agilent Technologies). The sequence encoding the short form of Xrp1 (Xrp1-S; amino acids 263-668) was PCR amplified from w^{1118} cDNA and cloned into the pENTR/D-TOPO vector using the following gene-specific primers: sense: 5'-CAC CAT GTT TGC CGA GGA GGA TCT GAT-3' and antisense 5'-TCA GTC CTG CTC CTG CTT AAC GTA AG-3' (with stop codon). To generate transgenic lines harboring the xrp1-L and xrp1-S coding sequences under the control of UAS (UAS-xrp1-L and UAS-xrp1-S), the pUASattB-xrp1-S and pUASattB-xrp1-L constructs were injected in the presence of the PhiC31 integrase and inserted into the 51C landing site on the 2nd chromosome.

QUANTIFICATION AND STATISTICAL ANALYSIS

P values are the result of ANOVA tests or Student's t-tests provided by GraphPad Prism (* $p<0.05$, ** $p<0.01$ and *** $p<0.001$). t-tests were used when two conditions were compared, and ANOVA for experiments comparing 3 or more conditions. Graphs were done using GraphPad Prism or Microsoft Excel. Single experiments were performed for Figures 1B, 1E, 2D, 3, 4A, S1, S2, S3, S4B. Two independent experiments were performed for Figures 1D, 2C, S4A.

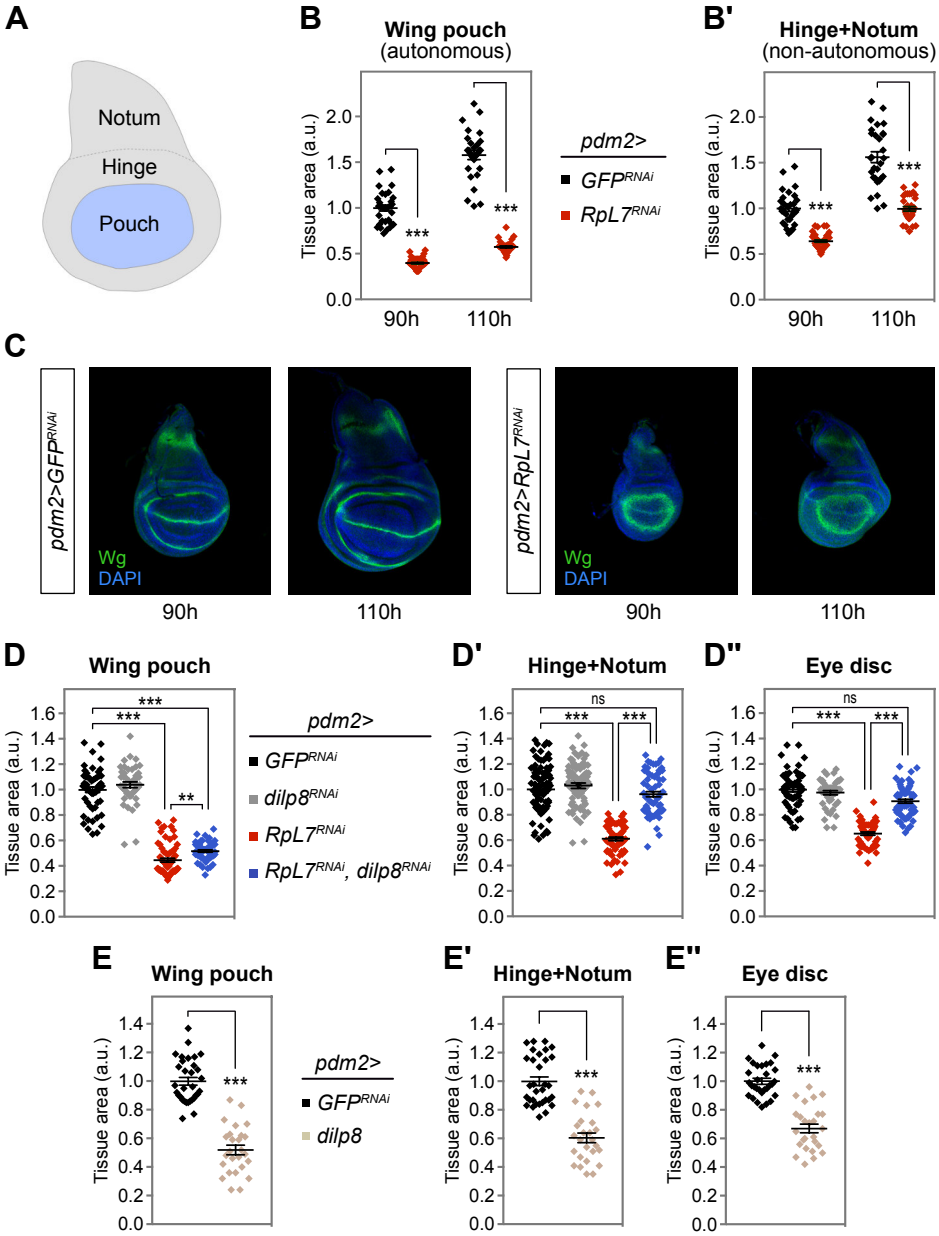
A
Notum
Hinge
Pouch
B
Wing pouch
(autonomous)
Tissue area (a.u.)
2.0
1.5
1.0
0.5
0.0
***
***
90h
110h
pdm2>
GFP^RNAi
RpL7^RNAi
B'
Hinge+Notum
(non-autonomous)
Tissue area (a.u.)
2.0
1.5
1.0
0.5
0.0
***
***
90h
110h
C
pdm2>GFP^RNAi
Wg
DAPI
90h
110h
pdm2>RpL7^RNAi
Wg
DAPI
90h
110h
D
Wing pouch
Tissue area (a.u.)
1.6
1.4
1.2
1.0
0.8
0.6
0.4
0.2
0.0
***
***
**
pdm2>
GFP^RNAi
dilp8^RNAi
RpL7^RNAi
RpL7^RNAi, dilp8^RNAi
D'
Hinge+Notum
Tissue area (a.u.)
1.6
1.4
1.2
1.0
0.8
0.6
0.4
0.2
0.0
ns
***
***
D''
Eye disc
Tissue area (a.u.)
1.6
1.4
1.2
1.0
0.8
0.6
0.4
0.2
0.0
ns
***
***
E
Wing pouch
Tissue area (a.u.)
1.4
1.2
1.0
0.8
0.6
0.4
0.2
0.0
***
pdm2>
GFP^RNAi
dilp8
E'
Hinge+Notum
Tissue area (a.u.)
1.4
1.2
1.0
0.8
0.6
0.4
0.2
0.0
***
E''
Eye disc
Tissue area (a.u.)
1.4
1.2
1.0
0.8
0.6
0.4
0.2
0.0
***

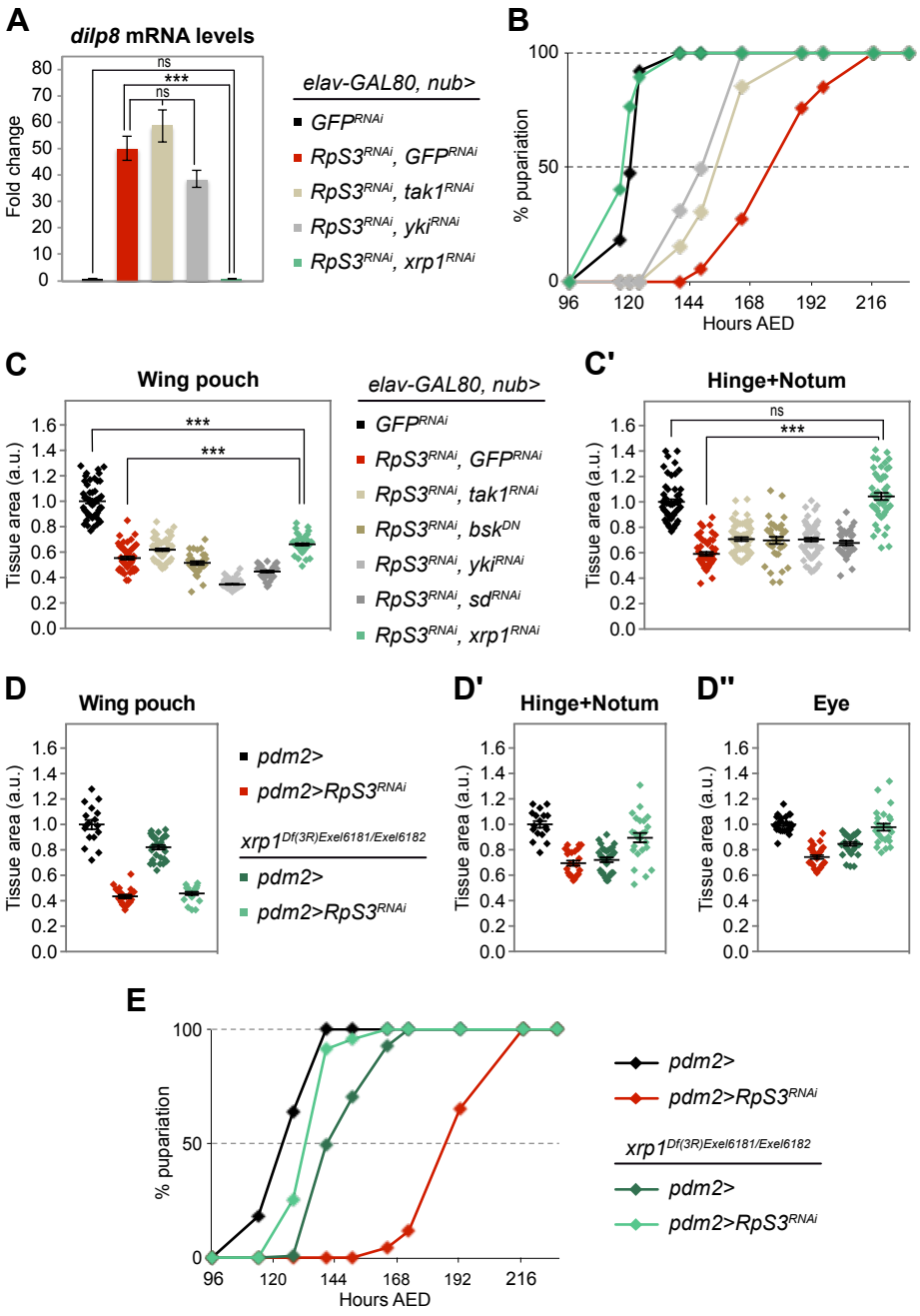
A
dilp8 mRNA levels
Fold change
ns
***
ns
elav-GAL80, nub>
GFP^RNAi
RpS3^RNAi, GFP^RNAi
RpS3^RNAi, tak1^RNAi
RpS3^RNAi, yki^RNAi
RpS3^RNAi, xrp1^RNAi
B
% pupariation
Hours AED
C
Wing pouch
Tissue area (a.u.)
RpS3^RNAi, bsk^DN
RpS3^RNAi, sd^RNAi
C'
Hinge+Notum
D
Wing pouch
pdm2>
pdm2>RpS3^RNAi
xrp1^Df(3R)Exel6181/Exel6182
D'
Hinge+Notum
D''
Eye
E

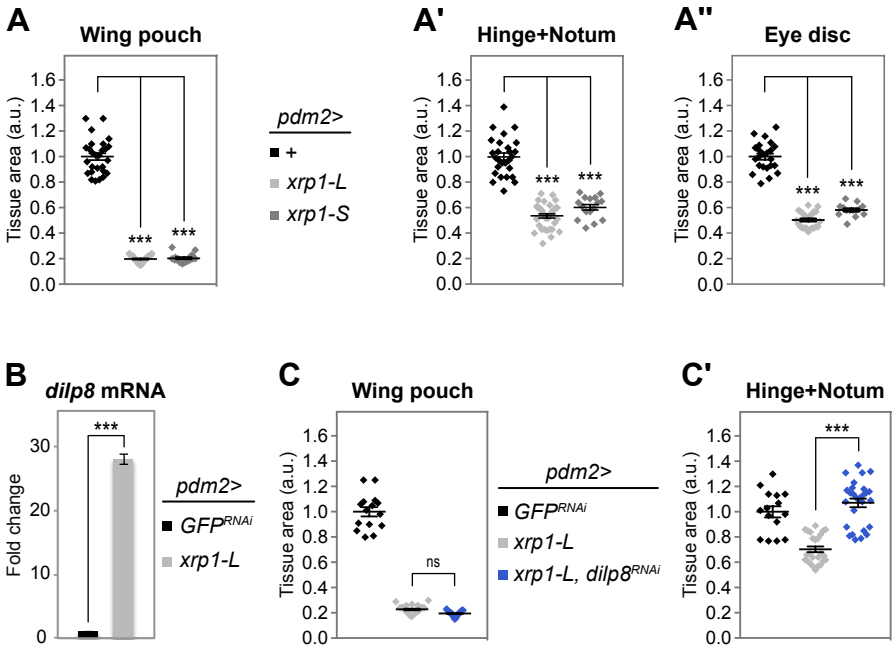
A
Wing pouch
Tissue area (a.u.)
1.6
1.4
1.2
1.0
0.8
0.6
0.4
0.2
0.0
***
***
pdm2>
+
xrp1-L
xrp1-S
A'
Hinge+Notum
A''
Eye disc

B
dilp8 mRNA
Fold change
30
20
10
0
***
pdm2>
GFP^RNAi
xrp1-L
C
Wing pouch
Tissue area (a.u.)
ns
pdm2>
GFP^RNAi
xrp1-L
xrp1-L, dilp8^RNAi
C'
Hinge+Notum

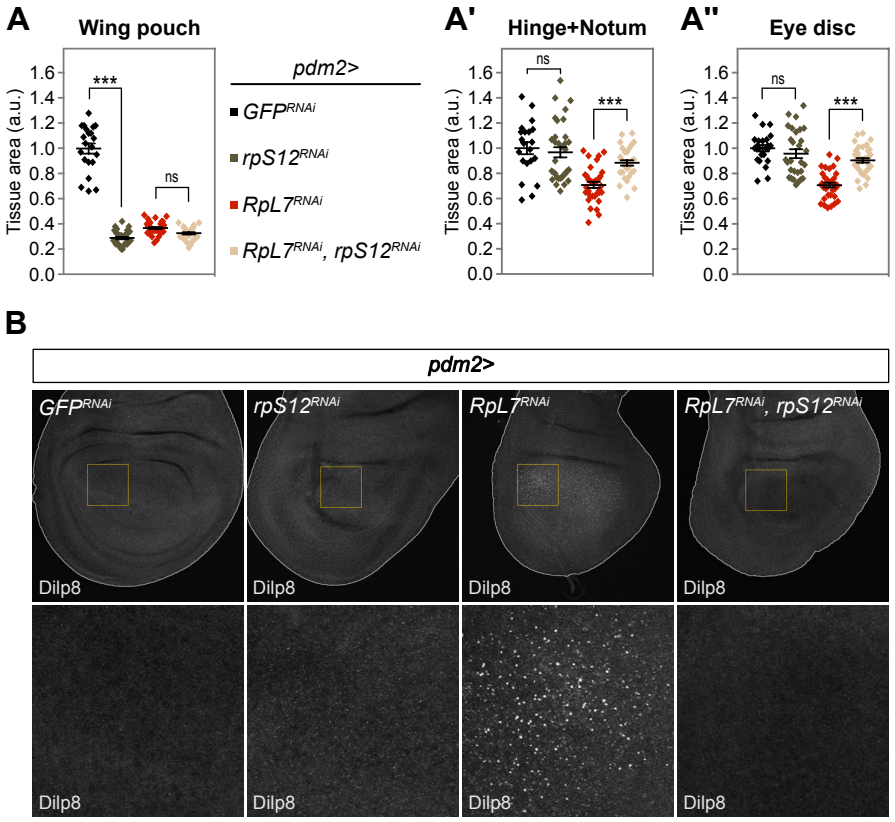
A
Wing pouch
A'
Hinge+Notum
A''
Eye disc
Tissue area (a.u.)
1.6
1.4
1.2
1.0
0.8
0.6
0.4
0.2
0.0
***
ns
pdm2>
GFP^RNAi
rpS12^RNAi
RpL7^RNAi
RpL7^RNAi, rpS12^RNAi
B
pdm2>
GFP^RNAi
rpS12^RNAi
RpL7^RNAi
RpL7^RNAi, rpS12^RNAi
Dilp8
C
Local growth inhibition/
Rp knock-down
RpS12
Xrp1
Dilp8
Ecdysone
Growth
(other domains)
Growth
(other discs)

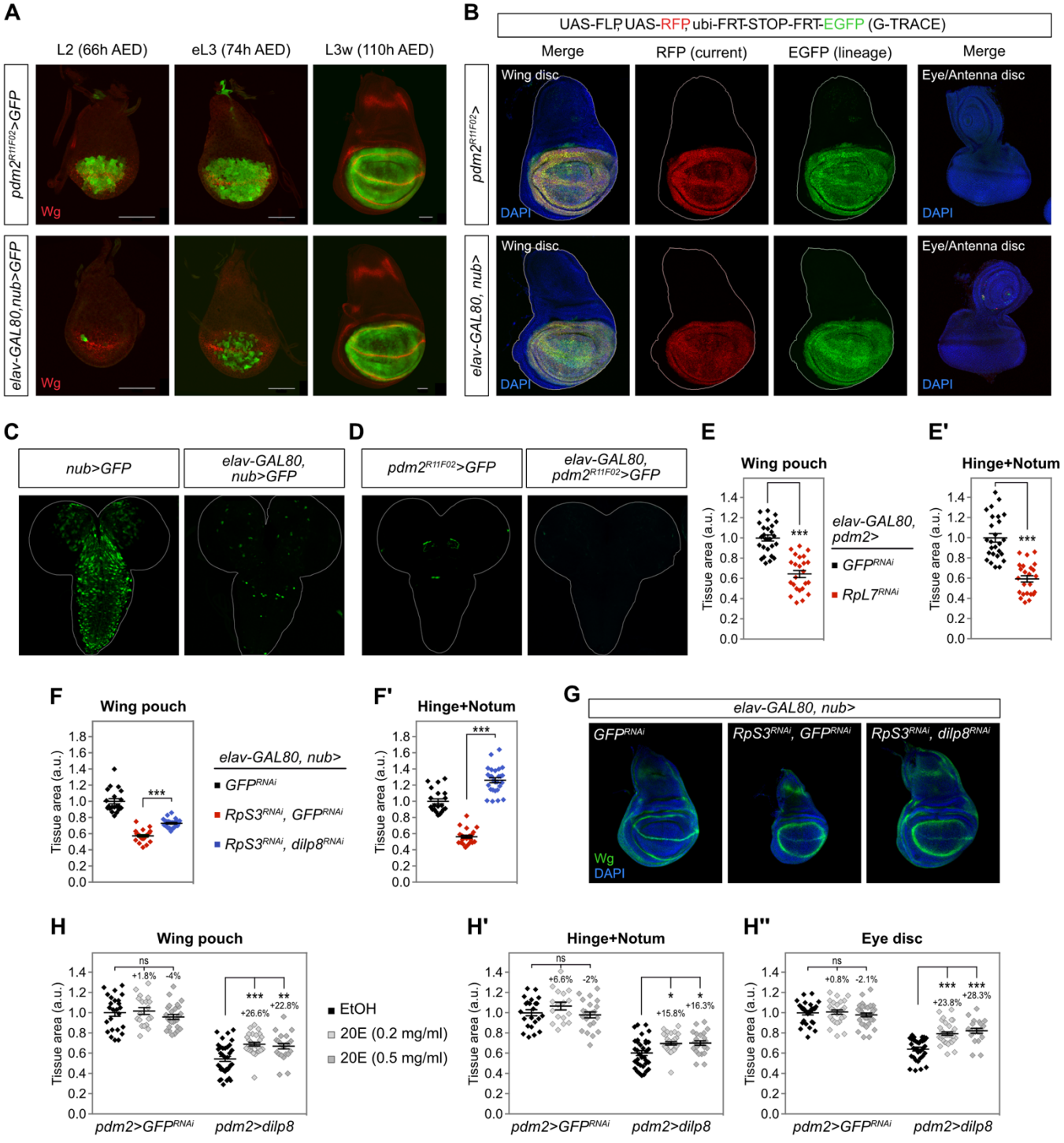

Figure S1, related to Figure 1

(A) Expression pattern of *pdm2*^{R11F02}*-Gal4* and *nub-Gal4* combined with an *elav-GAL80* construct (*elav-GAL80, nub>*) in wing imaginal discs at different stages of development (L2, second larval instar; eL3, early third instar; L3w, wandering third instar). (B) Lineage analysis using the G-TRACE technique revealing the expression pattern of *pdm2*^{R11F02}*-Gal4* and *elav-GAL80, nub-Gal4* drivers in wing and eye imaginal discs dissected at 110h AED. (C, D) Pictures of brains of the different genotypes at 110h

AE. (E, E') Measurement of wing pouch area (autonomous territory; E) and hinge and notum area (non-autonomous territories; E') showing the reduction of tissue size at 110h AED when *pdm2-Gal4* is combined with an *elav-GAL80* construct to drive *UAS-RpL7*^{RNAi} expression. Data are represented as mean ± SEM (n≥24; *** p<0.001, t-tests). (F, F') Measurement of wing pouch area (F) and hinge and notum area (F') in control wing discs (*elav-GAL80, nub>GFP*^{RNAi}), *Rp-RNAi* wing discs (*elav-GAL80, nub>RpS3*^{RNAi}*, GFP*^{RNAi}), and *Rp-RNAi* wing discs with the simultaneous knock-down of *dilp8* (*elav-GAL80, nub>RpS3*^{RNAi}*, dilp8*^{RNAi}). Experiments were done at 110h AED (n≥20). Data are represented as mean ± SEM (*** p<0.001, ANOVA) (G) Representative pictures of wing imaginal discs of the three genotypes stained for Wingless (Wg) illustrate the loss of coordination between the different territories in *elav-GAL80, nub>RpS3*^{RNAi}*, dilp8*^{RNAi} wing discs. (H-H'') Measurement of wing pouch area (H), area of neighboring territories (hinge and notum; H') and area of a remote organ (eye disc; H'') in control *pdm2>GFP*^{RNAi} animals and *pdm2>dilp8* animals at 110h AED, fed on medium supplemented either with ethanol (EtOH, control condition) or with two concentrations of 20E. Feeding animals 20E rescues the growth defects induced by *dilp8* overexpression in the pouch (n≥17). Data are represented as mean ± SEM (*** p<0.001, ** p<0.01, * p<0.05 and ns=not significant, ANOVA).

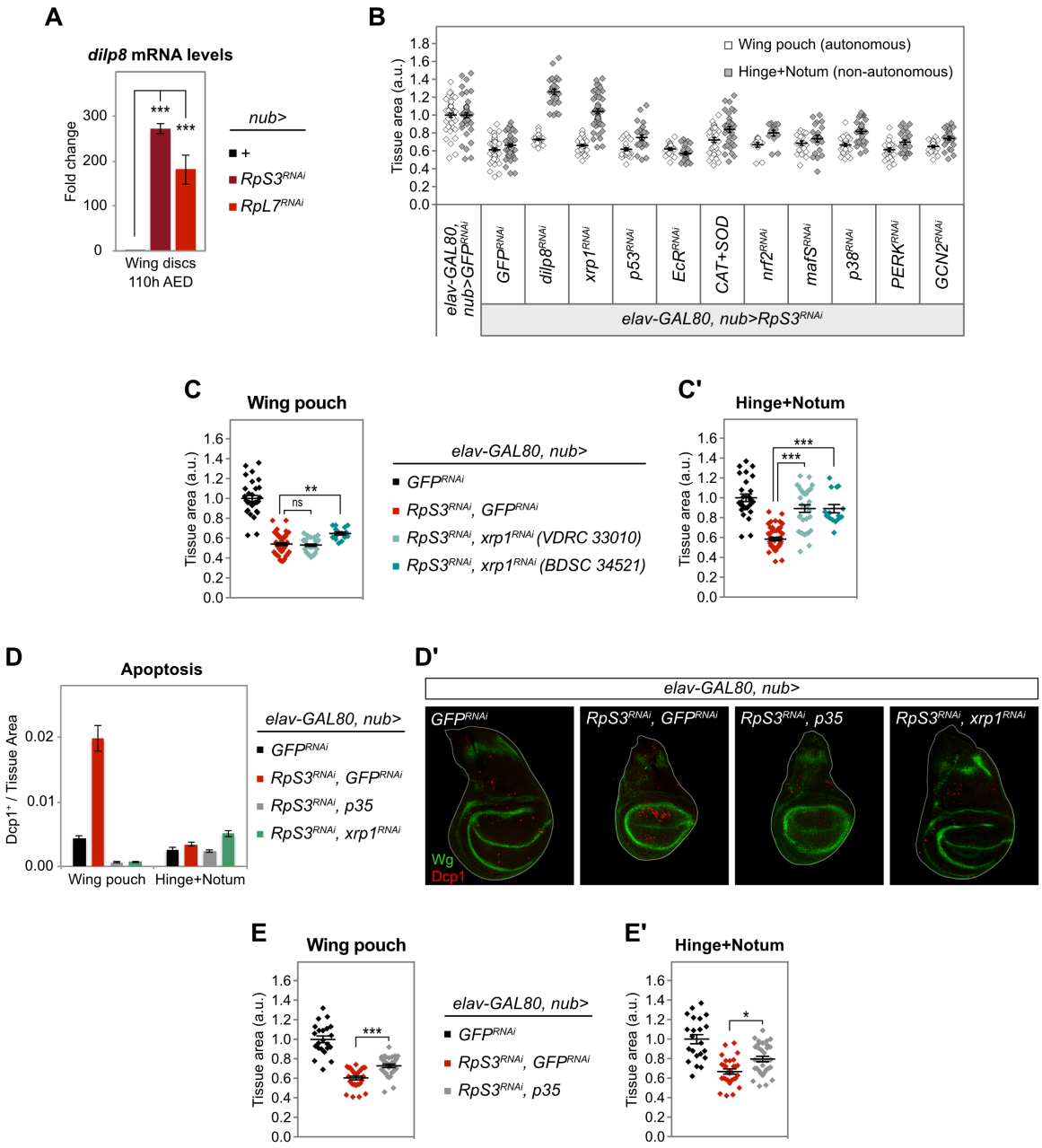

Figure S2, related to Figure 2

(A) Measurement of *dilp8* mRNA levels by qRT-PCR on dissected wing discs of the indicated genotypes at 110h AED. (B) Tissue area, expressed as a ratio to control (*elav-GAL80, nub>GFP^{RNAi}*), of the wing pouch and hinge+notum territories in the indicated genetic conditions. Experiments were done at 110h AED (n≥13). Data are represented as mean ± SEM. (C,C') Measurement of pouch area (C) and hinge and notum area (C') in wing discs of the indicated genotypes at 110h AED (n≥15), showing a rescue of the hinge+notum territories upon knock-down of *xrp1* in *Rp-RNAi* wing pouch. Data are represented as mean ± SEM (*** p<0.001, ** p<0.01 and ns=not significant, ANOVA). (D, D') Visualization of apoptosis in the wing pouch and hinge+notum area in wing discs of the indicated genotypes at 110h AED showing that apoptosis is rescued upon knock-down of *xrp1* in *Rp-RNAi* wing

pouch. (D) Quantification of apoptosis as measured by the ratio the fluorescent Dcp1-positive area and overall tissue area (pouch or hinge+notum, n≥22). (D') Representative pictures of wing discs of the different genotypes stained for Wingless and Dcp1. (E,E') Measurement of pouch area (E) and hinge and notum area (E') in wing discs of the indicated genotypes at 110h AED (n≥22). Blocking apoptosis by expressing *UAS-p35* has a very mild effect on tissue growth in *Rp-RNAi* wing discs. Data are represented as mean ± SEM (*** $p<0.001$ and * $p<0.05$, ANOVA).

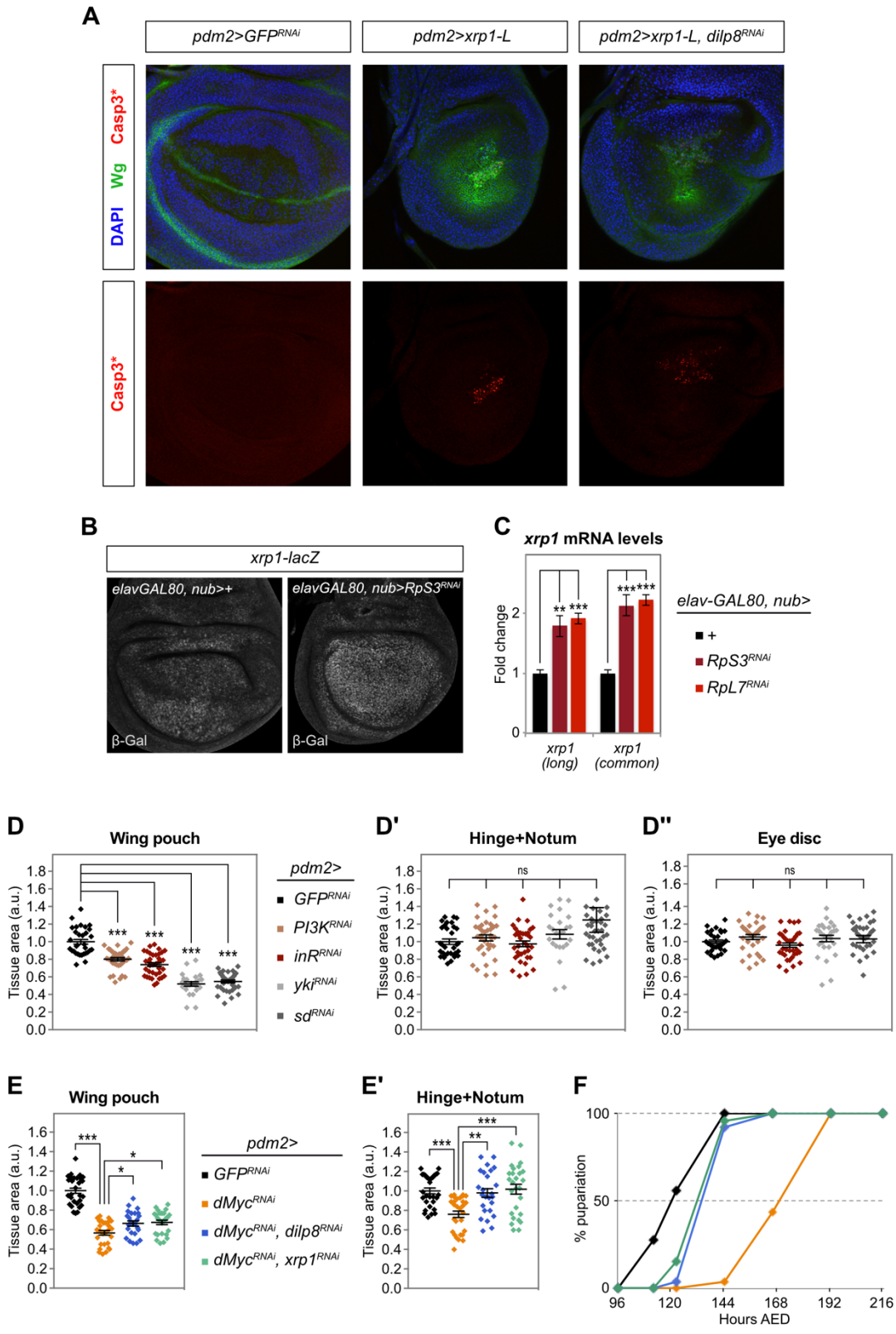

Figure S3, related to Figure 3

(A) Xrp1 overexpression induces cell death autonomously in a Dilp8-independent manner. Representative pictures of wing imaginal discs of the different genotypes stained for Wg and activated caspase 3 (Casp3*, indicative of cell death). (B) Activity of the *xrp1-lacZ* reporter in control and *Rp-RNAi* wing pouch. (C) *xrp1* mRNA levels measured by qRT-PCR on dissected wing discs of

control and *Rp-RNAi* discs. Experiments were done at 110h AED. Data are represented as mean ± SEM (** p <0.01 and *** p<0.001, ANOVA). (D-D'') Measurement of wing pouch area (D), area of neighboring territories (hinge and notum; D') and area of a remote organ (eye disc; D'') in animals of the indicated genotypes at 110h AED (n≥24). Data are represented as mean ± SEM (*** p<0.001 and ns=not significant, ANOVA). (E-E') Measurement of wing pouch area (E) and hinge and notum area (D') in wing discs of the indicated genotypes at 110h AED (n≥25), showing that the downregulation of *dilp8* or *xrp1* also rescues the undergrowth of the non-autonomous territories caused by the downregulation of *day* in the wing pouch (*pdm2>dMyc*^{RNAi} animals). Data are represented as mean ± SEM (*** p<0.001, ** p<0.01, * p<0.05 and ns=not significant, ANOVA). (F) Pupariation curve for animals of the genotypes indicated in (E). Percentage of larvae that have pupariated at the indicated hours AED is shown (n≥26).

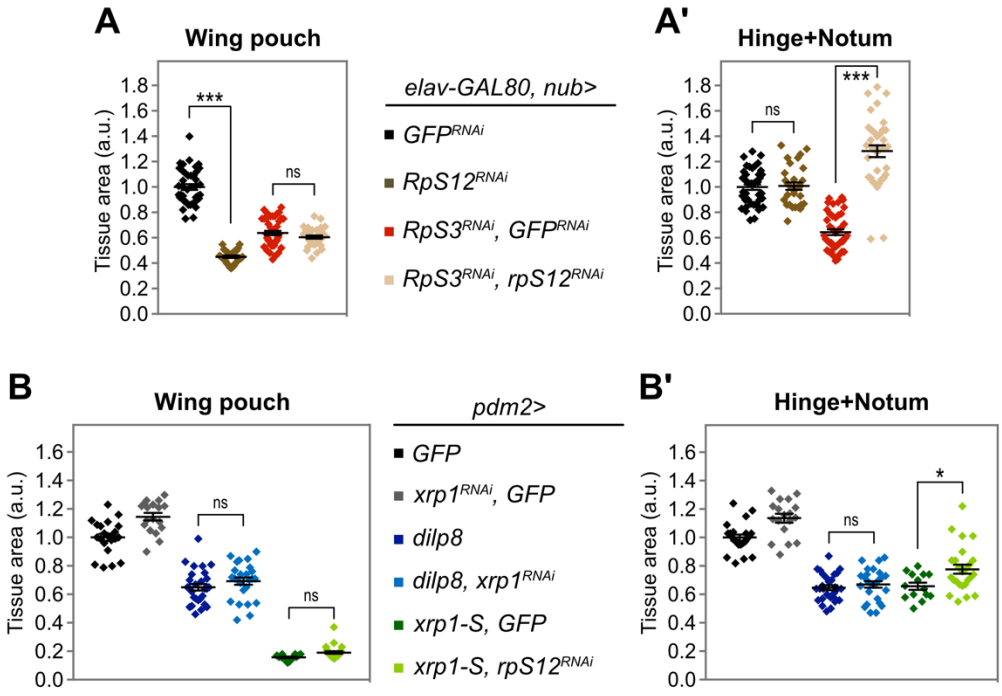

Figure S4, related to Figure 4

(A-A') Measurement of wing pouch area (A) and hinge and notum area (A') in control wing discs (*elav-GAL80, nub>GFP*^{RNAi}), wing discs with knock-down of *rpS12* (*elav-GAL80, nub>rpS12*^{RNAi}), *Rp-RNAi* wing discs (*elav-GAL80, nub>RpS3*^{RNAi}*, GFP*^{RNAi}), and *Rp-RNAi* wing discs with simultaneous knock-down of *rpS12* (*elav-GAL80, nub>RpS3*^{RNAi}*, rpS12*^{RNAi}). Experiments were done at 110h AED (n≥30). (B-B') Measurement of wing pouch area (A) and hinge and notum area (B') in animals of the indicated genotypes at 110h AED (n≥14). Data are represented as mean ± SEM (*** p<0.001, * p<0.05 and ns=not significant, ANOVA).

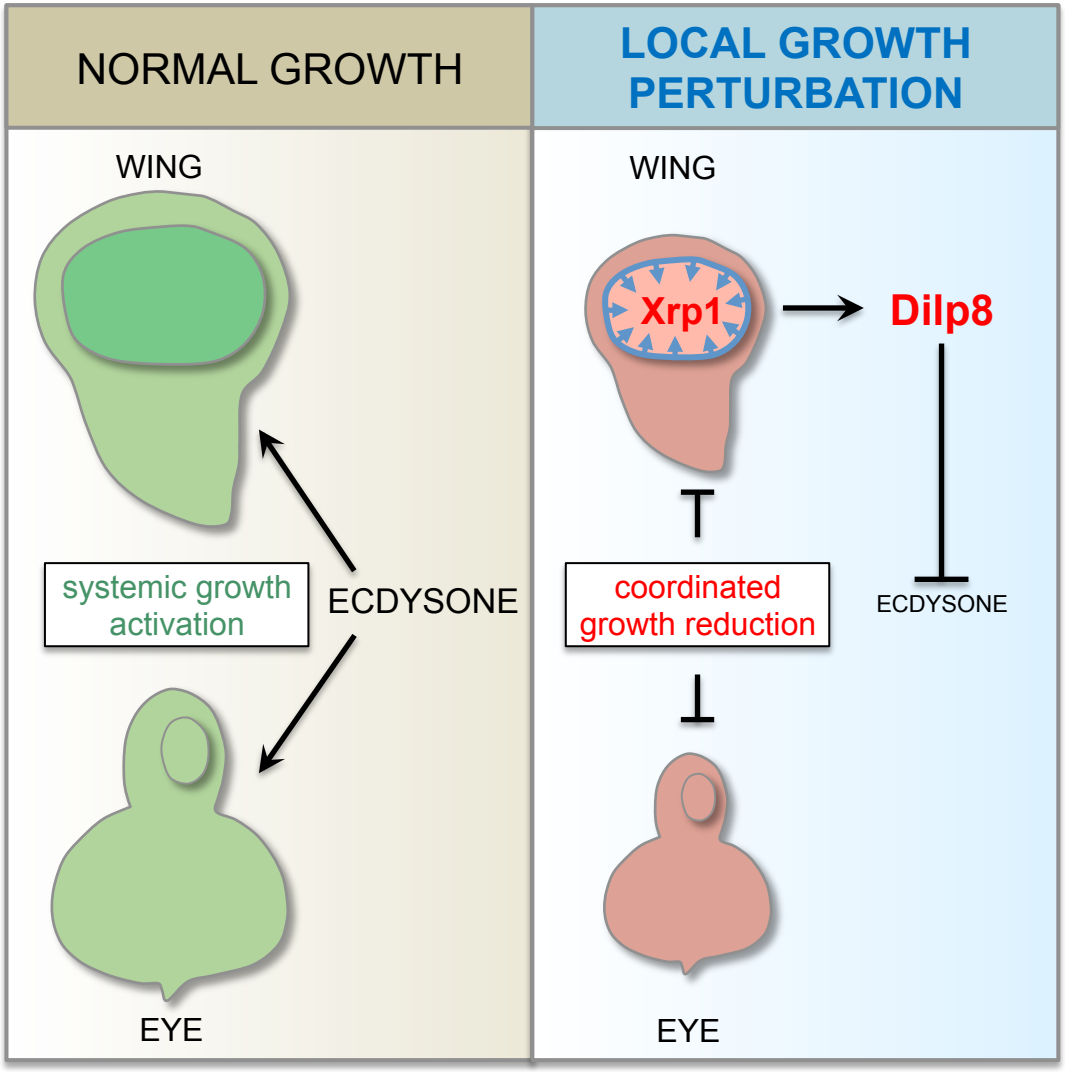
NORMAL GROWTH
LOCAL GROWTH PERTURBATION
WING
WING
Xrp1
Dilp8
systemic growth activation
ECDYSONE
coordinated growth reduction
ECDYSONE
EYE
EYE